ACS OMEGA

Open Access

http://pubs.acs.org/journal/acsodf

Article

Strategy for Patterning Titania Dendrites by Gas−Solution Interaction at Droplet Surfaces

Larisa B. Gulina,* Polina P. Senega, and Valeri P. Tolstoy

Cite This: *ACS Omega* 2023, 8, 33831−33837

Read Online

ACCESS | Metrics & More | Article Recommendations

ABSTRACT: Interaction of the solution droplet surface with gaseous components of the environment can lead to the formation of highly ordered patterns, such as dendrites. Here, we show that these structures can be spontaneously created during the open-air interaction of aqueous solution drop of titanium(III) salt with gaseous NH_3 at the contact boundary thereof. The conditions have been identified under which radially ordered dendritic patterns can form on the surface of the $TiCl_3$ solution droplet. The formation of these self-organized dendrite patterns can be attributed to the surface instability manifesting in Marangoni thermal flows in a droplet occurring during open-air fabrication. The composition of as-synthesized structures corresponds to coprecipitated crystalline NH_4Cl and amorphous TiO_2 nH_2O. After thermal treatment at 450 °C, TiO_2 with the anatase crystal lattice is formed; meanwhile, the ordered dendrite patterns are preserved.

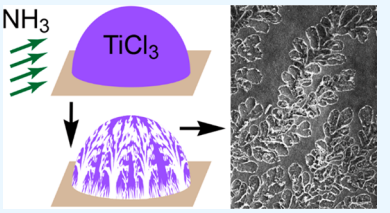

INTRODUCTION

The processes that occur during the formation, evaporation, and movement of a droplet attract great attention from researchers since they take place everywhere, in biology and inanimate nature, as well as in science and technology. These processes are widespread in microfluidics, lab-on-a-chip microsystems, additive manufacturing and printing, biochemical assays, and other applications.[1]

Studying the processes that occur in a drop and on its surface is necessary to understand the physicochemical features of self-organization of matter and to use them to create new materials. Recent works have focused on the investigation of colloidal droplet evaporation on a solid substrate and on the resulting formation of ordered patterns.[2,3] Evaporation-induced crystallization is observed with decreasing volume of a single or multicomponent solution droplet on the surface of a solid substrate.[4,5] The effect of surfactant on evaporation in a droplet is being studied.[6] The presence of a temperature gradient in a drop contributes to the occurrence of complicated, even fractal-like, deposit patterns.[7] The intermittent movement of the contact line during the droplet evaporation can lead to the appearance of single or multiple coffee rings.[8] In this work,[9] the diphenylalanine self-assembled microtubes have been grown via evaporation-driven crystallization, making use of the Marangoni flow in the drying droplets. The influence of a solid substrate surface geometry and wettability on the processes caused by droplet evaporation is being widely studied.[10−12] At the same time, there is a lack of studies that take into account the interaction of the droplet surface with the gaseous components of the environment, which occurs in both natural and industrial fields. Therefore, the study of specific physicochemical processes that take place on the solution droplet surface involving reagents in various aggregative states seems essential for getting new data regarding the substance self-organization processes occurring on the surface of a solution droplet under the action of a gaseous reagent.

Earlier, it was reported about obtaining ordered honeycomb-like manganese oxide structures on the surface of a drop of aqueous solution of manganese acetate under the action of gaseous ozone.[13,14] The object selected for the present research is the hydrated titanium dioxide formation reaction resulting from hydrolysis occurring on the surface of a drop of the titanium salt aqueous solution under the action of ammonia vapor in air. Titania has a range of promising multifunctional properties and a wide variety of applications in the creation of pigments,[15] sorbents,[16] catalysts,[17] optically and photochemically active materials,[18−20] sensors,[21] bactericidal[22] and smart[23,24] coatings, etc. Common methods for obtaining titania microspheres include hydrolysis between titanium alkoxide and water droplets in a microfluidic reactor[25] or thermally assisted hydrolysis of $TiCl_4$ vapors by water-based aerosol.[26] The study of sol−gel processes in a drop of titania ink was carried out in ref 27. A literature search in current sources found no information on the preparation of TiO_2 structures with dendritic morphology. Dendritic structures are known to have a large surface area and sharp crystal faces, so they are promising for catalytic and biosensor applications.[28]

Received: June 22, 2023
Accepted: August 28, 2023
Published: September 8, 2023

https://doi.org/10.1021/acsomega.3c04459
ACS Omega 2023, 8, 33831−33837

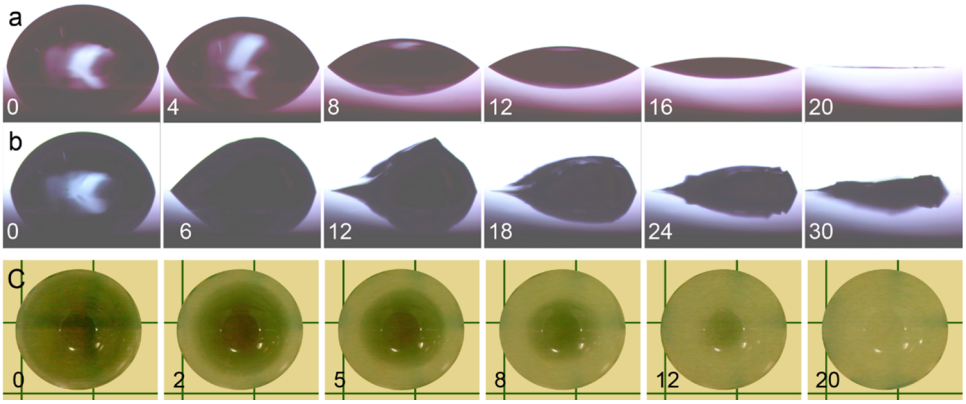

Figure 1. Optical images showing a $TiCl_3$ solution droplet evaporation in the open air (a) and in the presence of NH_3 vapors (b, c). The number in the lower left corner of each photo indicates the time (in seconds) from the beginning of observation.

The aim of this work is to study conditions for formation of dendritic structures based on titanium dioxide as a result of coprecipitation on the surface of an aqueous titanium(III) salt solution droplet under the action of gaseous NH_3 in an air atmosphere.

EXPERIMENTAL SECTION

Synthesis. The synthesis was carried out using $TiCl_3$ aqueous solutions prepared by diluting 15% titanium(III) chloride in hydrochloric acid (pure for analysis, ρ = 1.22 g/cm^3, from Lenreactiv) to a concentration of 0.001−0.2 mol/L. Ammonia gas source was a 25% solution of NH_3 H_2O (analytical grade, Lenreaktiv) diluted to a concentration of 5 M. All solutions were prepared using deionized water. Single-crystal silicon wafers of (111) orientation or glass microscope slides were used as substrates for the solution drop. Silicon wafers were etched in diluted HF (1:10 v/v) for 10 min, then washed in distilled water to remove the excess acid, and air-dried. To study peculiarities of the interaction occurring at the interface, a 0.1−10 μL drop of the solution was deposited on the Si wafer surface and placed in a reactor near the $NH_3{\cdot}H_2O$ diluted solution, which served as a gaseous reagent source. Using an optical microscope with 20−100× magnification, a goniometer, and video cameras, the process of the formation of a solid substance on the surface of a solution drop was observed for 15 min in situ. In this case, the droplet was filmed from two points: a top view and a side view.

Characterization. Morphology of the formed structures was studied by using optical and scanning electron microscopy (SEM) methods. To do this, we used an LK-1 goniometer (manufactured by the "Open Science", Russia), a Micromed optical microscope equipped with an Altami digital video camera, and a Zeiss EVO-40EP scanning electron microscope. The composition of the synthesized compounds was determined by using electron probe microanalysis (EPMA) with an INCA energy-dispersive X-ray spectrometry analyzer (EDX). The crystal structure of the reaction products on a single-crystal silicon substrate immediately after synthesis and after thermal treatment for 15 min at 450 °C was investigated by X-ray phase analysis (XRD). X-ray diffraction patterns of compounds on the surface of single-crystal silicon wafers were obtained by using a Bruker D2 Phaser diffractometer with a Cu Kα radiation source. Room-temperature Raman-scattering spectra were collected using a Confotec Uno confocal Raman spectrometer (SOL instruments) coupled with a ToupCam digital camera. The spectrometer was equipped with a 532 nm laser. The spot size of the laser on the samples was approximately 1 μm; the accumulation time was 5 s.

Photocatalysis. The photocatalytic activity of synthesized structures under sun irradiation was studied by the dye decomposition reaction of a methylene blue (MB) aqueous solution. Samples of photocatalysts were prepared as follows. Three 10 μL drops of 0.02 M $TiCl_3$ solution were deposited on the surface of single-crystal silicon wafers, and typical dendritic structures were formed under the action of NH_3 vapor. After annealing, these samples were designated as D-100 and D-450 in accordance with the treatment temperature. To prepare reference samples, 3 drops (V = 10 μL) of a colloidal suspension formed in a volume of 0.02 M $TiCl_3$ solution when adding the NH_3 H_2O solution, were deposited on the surface of Si wafers. After appropriate heat treatment, these samples were designated as S-100 and S-450. Each wafer with patterns was placed on the bottom of a flat container with 5 mL of a 5 mg/L MB solution. These containers were first aged for 30 min in the dark to check the absorption of dye onto the catalyst surface. After that, the solutions with the samples lying on the bottom were irradiated at a distance of 10 cm under daylight of 120 LED lamp (power 22 W, the color temperature corresponds to 5200 K) for 2 h. Every 30 min, the transmission spectrum of the dye solution was recorded on an SF-2000 spectrophotometer in the range of 400−800 nm. The ratio of the intensity of the absorbance peak at 665 nm before and after irradiation (I/I_0) was used to plot decomposition versus irradiation time and to calculate the catalyst efficiency.

RESULTS AND DISCUSSION

Evaporation of 3 μL droplet of 0.1 M $TiCl_3$ solution in air occurs while maintaining its radius, which can be seen from a series of successive photographs shown in Figure 1a. This effect is often observed when a small sessile droplet evaporates from a hydrophobic surface.[3,29,30] In the case of the environment containing ammonia vapor, a solid compound is precipitated on the droplet surface. Figure 1b shows photos of an evaporating drop of 0.1 M $TiCl_3$ solution in the presence of ammonia vapor, the drop of which was located at a 10 cm distance from the titanium(III) salt solution drop. It is clearly seen that the contour of the drop becomes asymmetric due to the salt precipitation on the droplet surface. Apart from this, the formed compound prevents the droplet evaporation, so that the process is not only slowed down but also becomes

https://doi.org/10.1021/acsomega.3c04459
ACS Omega 2023, 8, 33831−33837

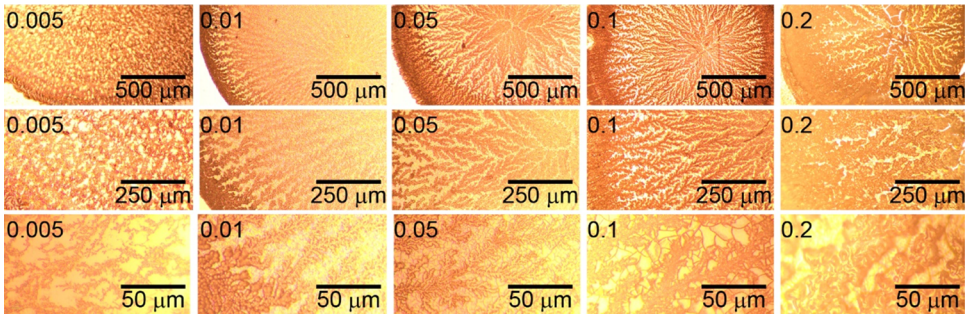

Figure 2. Optical photos at various magnifications of structures obtained by treatment of droplets of a $TiCl_3$ solution with gaseous NH_3. The solution concentration (C = 0.005−0.2 M) is shown in the upper left corner of each snapshot.

anisotropic. If a drop of $TiCl_3$ solution is placed in the center of a circle from NH_3 sources, then the ammonia vapor concentration around the droplet is practically the same. In this case, a solid formation starts at the line of triple contact between the gas, the solution, and the substrate surface, propagating from the droplet periphery to its top. Figure 1c shows a series of successive photos illustrating the change in the transparency of a 0.1 M $TiCl_3$ solution droplet in the presence of ammonia vapor when it acts on the drop simultaneously from all directions.

Images of patterns formed as a result of the contact of a drop of $TiCl_3$ solution of various concentrations with gaseous ammonia and the subsequent evaporation are shown in Figure 2. All patterns have a single clear contour, which confirms the fact that during evaporation of the treated droplet, its radius remains the same. Looking at a series of images obtained at the lowest magnification from left to right, one can observe an increase in the thickness of a denser ring located at the droplet periphery with an increasing concentration of the titanium salt solution. When dilute solutions are used, the main area of the pattern is formed by a network of filamentous structures with the thickness thereof somewhat decreasing from the drop periphery to its center. At a titanium salt solution concentration of 0.01 M and higher, dendritic structures are formed with growth direction coinciding with the droplet radius and the distribution density on the surface depends on the reagent concentration. According to our observations, at low solution concentrations in the droplet, the space between the dendritic structures remains free, so that the solution can evaporate freely. In more concentrated solutions, the space between the dendrites is a solid film, which is deformed upon a subsequent decrease in the droplet volume, forming characteristic folds or breaks.

The study of pattern composition carried out by EPMA showed that the Ti/Cl ratio is lower at the droplet periphery than it is at its center (Figure 3). Thus, the EDX spectrum obtained at the pattern edge corresponds to the ratio Ti/Cl = 2:3, and the spectrum of the central region corresponds to Ti/Cl = 3:1. These data suggest that crystallization begins with the NH_4Cl salt formation, but during the growth of dendrites, along with the increasing pH of the solution, the Cl content in the precipitate decreases, while the Ti content increases. It is important that after thermal treatment of the obtained dendritic structures, the composition thereof on the substrate surface corresponds to titanium dioxide due to the ammonium salt decomposition.

The latter fact is confirmed by the results of the X-ray phase analysis of patterns on the single-crystal silicon surface (Figure 4a). Immediately after synthesis, the X-ray diffraction pattern contains only the maxima related to cubic NH_4Cl crystals.[31]

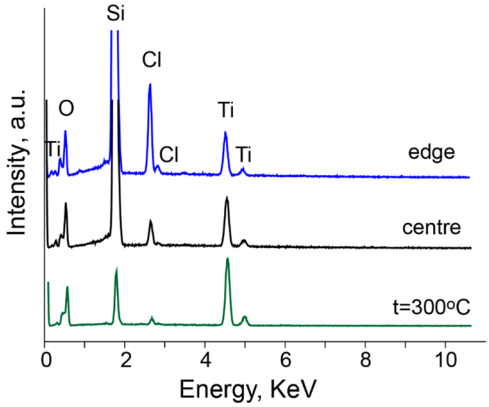

Figure 3. EPMA spectra in different regions of drop pattern on a Si substrate after synthesis and annealing at 300 °C.

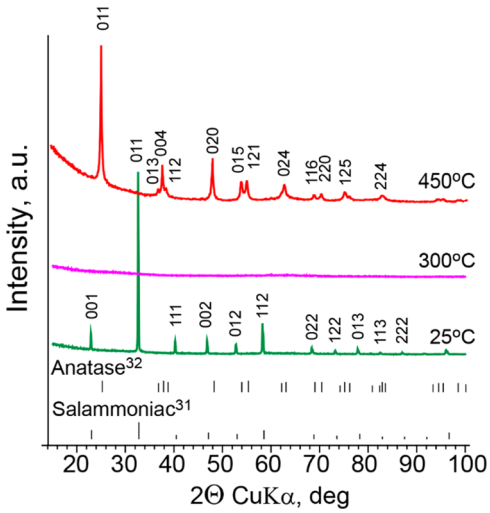

Figure 4. X-ray diffraction patterns of dendrite structures on a silicon surface after synthesis (green) and annealing at 300 °C (purple) and 450 °C (red). Black marks—data for NH_4Cl[31] and TiO_2.[32]

After heat treatment at T = 300 °C with the ammonium salt decomposition, the X-ray pattern demonstrates the formation of an amorphous compound, which acquires the anatase structure[32] as a result of heat treatment at 450 °C.

Raman spectra of dendrite structures on a glass support are presented in Figure 5. The spectrum of structures immediately

https://doi.org/10.1021/acsomega.3c04459
ACS Omega 2023, 8, 33831−33837

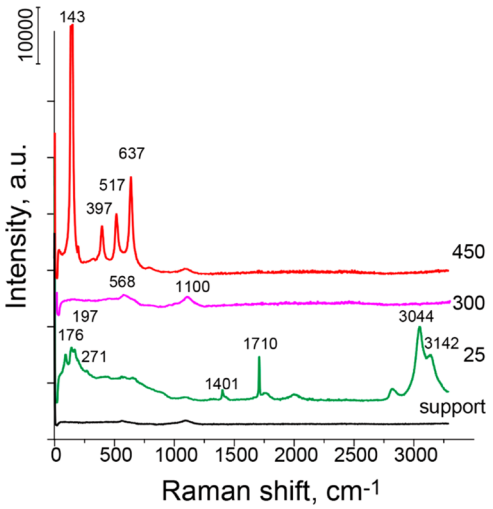

Figure 5. Raman spectra of dendrite structures on a glass support after synthesis and after annealing at 300 and 450 °C.

after synthesis has four fundamental Raman-active modes related to the NH_4^+ group:[33] vibrational ν_1 symmetric stretch at 3044 cm^{-1}, ν_2 in-plane bend at 1710 cm^{-1}, ν_3 asymmetric stretch at 3142 cm^{-1}, and ν_4 out-of-plane bend at 1401 cm^{-1}. These maxima, as well as those at 271 and 176 cm^{-1}, correspond to transverse and longitudinal frequencies of NH_4Cl modes.[34] After annealing at 300 °C, the characteristic Raman shift values of NH_4Cl disappear and the spectrum characterizes the amorphous state of the product on the substrate surface. Weak maxima at 1100 and 565 cm^{-1} coincide with the maxima characteristic of an amorphous glass microscope slide[35] observed on the spectra of a clean substrate. After heating the sample at 450 °C, maxima at 143, 397, 517, and 637 cm^{-1} are observed, which can be related to the characteristic Raman-active modes of anatase TiO_2 with symmetries E_g, B_{1g}, A_{1g}, and E_g correspondingly.[36]

Figure 6 shows SEM images of dendritic structures immediately after the synthesis and after thermal treatment. It can be seen that the dendritic structures consist of an array of hollow spherical formations (Figure 6a,b). The capsule wall thickness does not exceed 100 nm (Figure 6c). As a result of heating at a temperature of 300 °C, the walls of the capsule become thinner and "open", which can be seen in Figure 6d,e. This process is caused by the ammonium salt decomposition. Figure 6f clearly shows that the capsule wall consists of amorphous nanoparticles, and this is in line with the XRD data. Upon heat treatment at 450 °C, despite the phase transition of titanium dioxide from the amorphous to crystalline state with the anatase structure, the product morphology practically does not change. The images in Figure 6g,h clearly show the preserved pattern of dendrites consisting of TiO_2 nanoparticles. As can be seen from Figure 6i, the size of each particle is about 20 nm.

Based on the presented results, we can suggest the following model for the formation of dendrites on the surface of a solution droplet. The action of gaseous ammonia at the point of contact of a strongly acidic solution of titanium salt with the substrate surface initiates the formation of cubic NH_4Cl crystals. This observation is in agreement with the data[37] that two-dimensional crystallization at the liquid−gas interface starts at the point of contact with a solid. The formation of dendritic structures is often observed during the crystallization of NH_4Cl.[38] Another factor contributing to the formation of patterns is the diffusion−kinetic nature of the interaction. It is known, for instance, that the diffusion rate during the NaCl crystal growth in a gel matrix determines a variety of 2D dendritic morphologies, such as orthogonal or oblique lattices and curved weaves.[39] Similar entanglements of cubic crystals are observed at high solution concentrations at the droplet periphery. Since ammonia vapor tends to rise upward, the direction of growth of dendritic structures coincides with the radial direction, and the density of distribution thereof on the

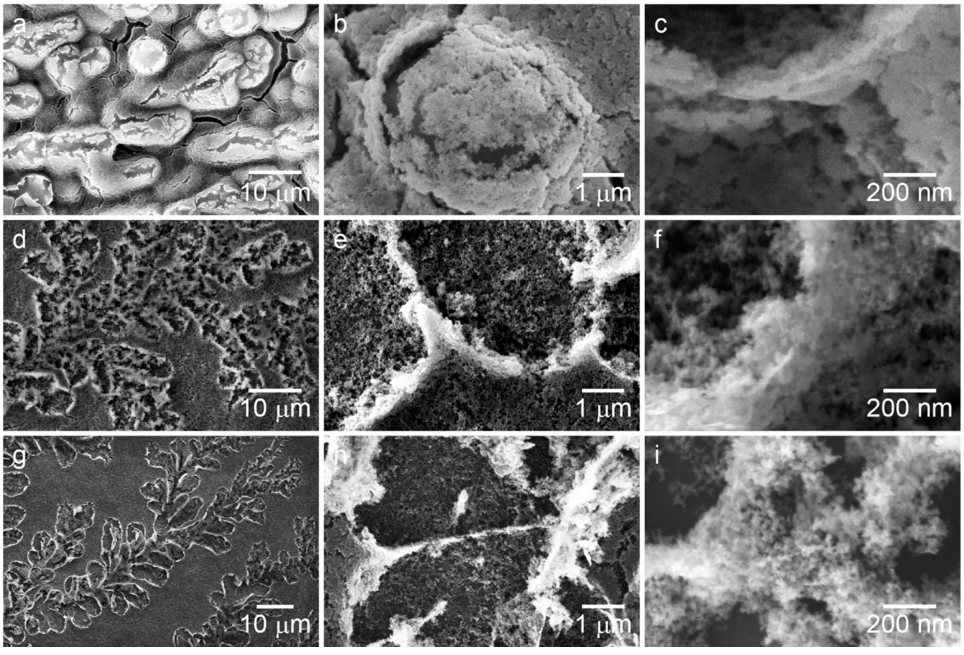

Figure 6. SEM images of the structures obtained by treating a 0.02 M $TiCl_3$ solution droplet with gaseous NH_3 at various magnifications after drying in air at room temperature (a−c) and after annealing at 300 °C (d−f) and 450 °C (g−i).

https://doi.org/10.1021/acsomega.3c04459
ACS Omega 2023, 8, 33831−33837

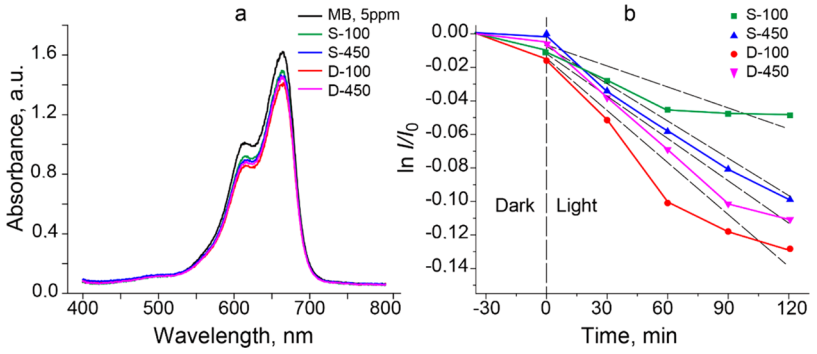

Figure 7. Absorption spectra of MB solutions before and after catalytic action (a). Evaluation of the decomposition efficiency ln I/I_0 at a wavelength of λ = 665 nm depending on the reaction time (b).

droplet surface is determined primarily by the concentration of the titanium salt solution. It can also be assumed that at the initial instant of time, titanium(III) hydroxide coprecipitates together with NH_4Cl, as evidenced by the distinctive purple hue shade of the drop seen in the first images of Figure 1c. However, in the presence of atmospheric oxygen, titanium(III) hydroxide is easily oxidized to hydrated titanium dioxide, which explains the change in the droplet color in the images on the right side of Figure 1c. This is how dendritic structures composed of $NH_4Cl/TiO_2{\cdot}H_2O$ are formed.

At thermal treatment due to the removal of moisture and ammonium salt decomposition, characteristic patterns consisting of TiO_2 nanoparticles are formed. Perhaps, this approach of "sacrificial" cocrystallization on the droplet surface can be possibly used to obtain dendrites of other oxides, those that cannot have a similar morphology when synthesized by traditional methods.

Figure 7 shows the results of evaluation of the photocatalytic activity of the synthesized samples with the morphology of dendritic structures after heating thereof at temperatures of 100 and 450 °C, designated as D-100 and D-450, respectively. The reference samples were the prints obtained after drying the drops of titanium dioxide particle suspension obtained by adding the ammonia solution to the $TiCl_3$ salt solution; the samples were designated as S-100 and S-450 in accordance with thermal treatment mode. The concentration of the titanium salt solution in all experiments was the same, that is, 0.02 M, and the droplet volume was 10 μL. It can be seen that, as a result of the dye sorption first stage carried out in the dark, the optical density of dye solutions changes more in samples with a low treatment temperature than in those annealed, and no dependence on the print preparation method is observed. Based on the results of a 2 h observation, it can be concluded that the photocatalytic activity of patterns obtained using suspension drops is generally lower than that of dendritic structural patterns. This can be explained by the unique morphology of the dendritic structures by analogy with ref 40, which found that ordering improves photocatalytic response. An unexpected result is the highest activity of a sample of dendritic structures dried at a temperature of 100 °C. According to XRD and microanalysis data, this sample contains ammonium salt crystals and titanium dioxide amorphous particles, while its increased catalytic activity can be due, on the one hand, to morphological features and, on the other hand, to an increased content of Brönsted and Lewis acid sites on the surface.

It is also important to emphasize that despite the relatively low absolute values of the change in the optical density of the solution, the decomposition of 5 mL of the dye was carried out using trace amounts of the active substance, which, in all cases, were less than 0.2 mg. This value is significantly less than the weights of catalysts based on titanium dioxide, which are usually used to study photocatalytic decomposition reactions.

CONCLUSIONS

In the presence of ammonia vapor on the surface of a drop of hydrochloric acid solution $TiCl_3$ with a concentration of 0.01−0.2 M, dendritic structures of a solid are formed on its surface. The dendrites start to grow along the line of the triple contact of the gas, liquid, and solid substrate; the growth is directed toward the droplet's top. After evaporation of the solution in air, patterns with the characteristic morphology of radially ordered dendritic structures consisting of hollow capsules are formed on the substrate. The chemical composition of the structures corresponds to a mixture of crystalline NH_4Cl and amorphous $TiO_2{\cdot}nH_2O$ coprecipitating together. After annealing at a temperature of 300 °C and upon decomposition of the ammonium salt, the dendrite composition corresponds to amorphous titanium dioxide, which converts to anatase as a result of heat treatment at 450 °C.

The obtained experimental results will be useful for studying 3D printing processes and the functioning of self-cleaning surfaces and membranes in microfluidics; these results are important for the development of innovative approaches to the creation of miniature sensors and devices. Moreover, the strategy for obtaining dendritic patterns developed on the basis of coprecipitation of salts on the surface of a solution droplet can be extended to a wide range of compounds and contributes to the production of new materials with a unique morphology.

AUTHOR INFORMATION

Corresponding Author

Larisa B. Gulina − *Saint-Petersburg State University, St. Petersburg 199034, Russia;* orcid.org/0000-0002-1622-4311; Email: l.gulina@spbu.ru

Authors

Polina P. Senega − *Saint-Petersburg State University, St. Petersburg 199034, Russia*

Valeri P. Tolstoy − *Saint-Petersburg State University, St. Petersburg 199034, Russia*

Complete contact information is available at: https://pubs.acs.org/10.1021/acsomega.3c04459

https://doi.org/10.1021/acsomega.3c04459
ACS Omega 2023, 8, 33831−33837

Author Contributions

The manuscript was written through contributions of all authors. L.B.G. designed the study, analyzed the experiment and wrote the paper, P.P.S. carried out the video recording of the droplet evaporation, V.P.T. performed SEM and EDX measurements. All authors have given approval to the final version of the manuscript.

Funding

This work was supported by the Russian Science Foundation (Project No. 22-29-00687, https://www.rscf.ru/project/22-2900687/).

Notes

The authors declare no competing financial interest.

■ ACKNOWLEDGMENTS

The synthesized samples were studied at the Resource Center for X-ray Diffraction Studies, and the Interdisciplinary Center for Nanotechnologies, St. Petersburg State University.

■ REFERENCES

(1) Lathia, R.; Nampoothiri, K. N.; Sagar, N.; Bansal, S.; Modak, C. D.; Sen, P. Advances in Microscale Droplet Generation and Manipulation. *Langmuir* **2023**, *39*, 2461−2482.
(2) Li, Y.; Salvator, V.; Wijshoff, H.; Versluis, M.; Lohse, D. Evaporation-Induced Crystallization of Surfactants in Sessile Multicomponent Droplets. *Langmuir* **2020**, *36*, 7545−7552.
(3) Yang, X.; Wu, M.; Doi, M.; Man, X. Evaporation Dynamics of Sessile Droplets: The Intricate Coupling of Capillary, Evaporation, and Marangoni Flow. *Langmuir* **2022**, *38*, 4887−4893.
(4) Wang, Z.; Orejon, D.; Takata, Y.; Sefiane, K. Wetting and evaporation of multicomponent droplets. *Phys. Rep.* **2022**, *960*, 1−37.
(5) Hong, M. S.; Lu, A. E.; Bae, J.; Lee, J. M.; Braatz, R. D. Droplet-Based Evaporative System for the Estimation of Protein Crystallization Kinetics. *Cryst. Growth Des.* **2021**, *21*, 6064−6075.
(6) Ildefonso, M.; Candoni, N.; Veesler, S. Heterogeneous Nucleation in Droplet-Based Nucleation Measurements. *Cryst. Growth Des.* **2013**, *13*, 2107−2110.
(7) Breid, D.; Lai, V.; Flowers, A. T.; Guan, X.; Liu, Q.; Velankar, S. S. Drop Spreading and Confinement in Swelling-Driven Folding of Thin Films. *Langmuir* **2021**, *37*, 6985−6994.
(8) Zhang, W.; Yu, T.; Liao, L.; Cao, Z. Ring formation from a drying sessile colloidal droplet. *AIP Adv.* **2013**, *3*, No. 102109.
(9) Nuraeva, A.; Vasilev, S.; Vasileva, D.; Zelenovskiy, P.; Chezganov, D.; Esin, A.; Kopyl, S.; Romanyuk, K.; Shur, V. Y. K.; Andrei, L. Evaporation-Driven Crystallization of Diphenylalanine Microtubes for Microelectronic Applications. *Cryst. Growth Des.* **2016**, *16*, 1472−1479.
(10) Gao, S.; Long, J.; Liu, W.; Liu, Z. Evaporation-Induced Wetting Transition of Nanodroplets on Nanopatterned Surfaces with Concentric Rings: Surface Geometry and Wettability Effects. *Langmuir* **2019**, *35*, 9546−9553.
(11) Kumar, A.; Sen, D.; Das, A.; Bahadur, J. Pattern of an Evaporated Colloidal Droplet on a Porous Membrane Dictated by Competitive Processes of Flow and Absorption. *Langmuir* **2022**, *38*, 7121−7128.
(12) Boinovich, L.; Emelyanenko, A. M.; Korolev, V. V.; Pashinin, A. S. Effect of Wettability on Sessile Drop Freezing: When Superhydrophobicity Stimulates an Extreme Freezing Delay. *Langmuir* **2014**, *30*, 1659−1668.
(13) Tolstoy, V. P.; Vladimirova, N. I.; Gulina, L. B. Ordered honeycomb-like network of MnO2·nH2O nanocrystals formed on the surface of a Mn(OAc)2 solution drop upon interaction with O3 gas. *Mendeleev Commun.* **2019**, *29*, 713−715.
(14) Tolstoy, V. P.; Vladimirova, N. I.; Gulina, L. B. Formation of ordered honeycomb-like structures of manganese oxide 2D nanocrystals with the birnessite-like structure and their electrocatalytic properties during oxygen evolution reaction upon water splitting in an alkaline medium. *ACS Omega* **2019**, *4*, 22203−22208.
(15) Amorim, S. M.; Suave, J.; Andrade, L.; Mendes, A. M.; José, H. J.; Moreira, R. F. P. M. Towards an efficient and durable self-cleaning acrylic paint containing mesoporous TiO2 microspheres. *Prog. Org. Coat.* **2018**, *118*, 48−56.
(16) Xu, Y.; Tay, T. F.; Cui, L.; Fan, J.; Niu, C.; Chen, D.; Guo, Z. X.; Sun, C.; Zhang, X. L.; Caruso, R. A. Trace-Level Fluorination of Mesoporous TiO(2) Improves Photocatalytic and Pb(II) Adsorbent Performances. *Inorg. Chem.* **2020**, *59*, 17631−17637.
(17) Chen, X.; Mao, S. S. Titanium dioxide nanomaterials: Synthesis, properties, modifications and applications. *Chem. Rev.* **2007**, *107*, 2891−2959.
(18) Marchuk, M. V.; Asanov, I. P.; Panafidin, M. A.; Vorotnikov, Y. A.; Shestopalov, M. A. Nano TiO2 and Molybdenum/Tungsten Iodide Octahedral Clusters: Synergism in UV/Visible-Light Driven Degradation of Organic Pollutants. *Nanomaterials* **2022**, *12*, 4282.
(19) Minnekhanov, A.; Kytina, E.; Konstantinova, E.; Kytin, V.; Marikutsa, A.; Elizarov, P. Photoinduced Dynamics of Radicals in N- and Nb-Codoped Titania Nanocrystals with Enhanced Photocatalysis: Experiment and Modeling. *Cryst. Growth Des.* **2022**, *22*, 4288−4297.
(20) Khamova, T. V.; Kopitsa, G. P.; Nikolaev, A. M.; Kovalenko, A. S.; Panova, G. G.; Udalova, O. R.; Zhuravleva, A. S.; Gorshkova, Y. E.; Chelibanov, V. P.; Chelibanov, I. V.; Baranchikov, A. E.; Tsvigun, N. V.; Pipich, V.; Shilova, O. A. The structure and properties of TiO2 nanopowders for use in agricultural technologies. *Biointerface Res. Appl. Chem.* **2021**, *11*, 12285−12300.
(21) Mokrushin, A. S.; Simonenko, E. P.; Simonenko, N. P.; Akkuleva, K. T.; Antipov, V. V.; Zaharova, N. V.; Malygin, A. A.; Bukunov, K. A.; Sevastyanov, V. G.; Kuznetsov, N. T. Oxygen detection using nanostructured TiO2 thin films obtained by the molecular layering method. *Appl. Surf. Sci.* **2019**, *463*, 197−202.
(22) Yamaguchi, M.; Abe, H.; Ma, T.; Tadaki, D.; Hirano-Iwata, A.; Kanetaka, H.; Watanabe, Y.; Niwano, M. Bactericidal Activity of TiO2 Nanotube Thin Films on Si by Photocatalytic Generation of Active Oxygen Species. *Langmuir* **2020**, *36*, 12668−12677.
(23) Ohko, Y.; Tatsuma, T.; Fujii, T.; Naoi, K.; Niwa, C.; Kubota, Y.; Fujishima, A. Multicolour photochromism of TiO2 films loaded with silver nanoparticles. *Nat. Mater.* **2003**, *2*, 29−31.
(24) Chen, X.; Zhang, Y.; Wu, B.; Sant, G. A Nitrogen- and Self-Doped Titania Coating Enables the On-Demand Release of Free Radical Species. *ACS Omega* **2019**, *4*, 18567−18573.
(25) Gong, X.; Wang, L.; Wen, W. Design and fabrication of monodisperse hollow titania microspheres from a microfluidic droplet-template. *Chem. Commun.* **2009**, *2009* (31), 4690−4692.
(26) Tarasov, A.; Trusov, G.; Minnekhanov, A.; Gil, D.; Konstantinova, E.; Goodilin, E.; Dobrovolsky, Y. Facile preparation of nitrogen-doped nanostructured titania microspheres by a new method of Thermally Assisted Reactions in Aqueous Sprays. *J. Mater. Chem. A* **2014**, *2*, 3102−3109.
(27) Yakovlev, A. V.; Milichko, V. A.; Pidko, E. A.; Vinogradov, V. V.; Vinogradov, A. V. Inkjet printing of TiO2/AlOOH heterostructures for the formation of interference color images with high optical visibility. *Sci. Rep.* **2016**, *6*, No. 37090.
(28) Bahadori, S. R.; Mei, L.; Athavale, A.; Chiu, Y.-j.; Pickering, C. S.; Hao, Y. New Insight into Single-Crystal Silver Dendrite Formation and Growth Mechanisms. *Cryst. Growth Des.* **2020**, *20*, 7291−7299.
(29) Erbil, H. Y. Evaporation of pure liquid sessile and spherical suspended drops: A review. *Adv. Colloid Interface Sci.* **2012**, *170*, 67−86.
(30) Birdi, K. S.; Vu, D. T.; Winter, A. A study of the evaporation rates of small water drops placed on a solid surface. *J. Phys. Chem. A* **1989**, *93*, 3702−3703.
(31) Bartlett, G.; Langmuir, I. The crystal structures of the ammonium halides above and below the transition temperatures. *J. Am. Chem. Soc.* **1921**, *43*, 84−91.
(32) Horn, M.; Schwerdtfeger, C. F.; Meagher, E. P. Refinement of the structure of anatase at several temperatures. *Z. Kristallogr.* **1972**, *136*, 273−281.

https://doi.org/10.1021/acsomega.3c04459
ACS Omega 2023, 8, 33831−33837

(33) Fastelli, M.; Comodi, P.; Maturilli, A.; Zucchini, A. Reflectance Spectroscopy of Ammonium Salts: Implications for Planetary Surface Composition. *Minerals* **2020**, *10*, 902.
(34) Fredrickson, L. R.; Decius, J. C. The Raman spectrum of the ordered phase of NH4Cl and ND4Cl: Dipole and polarizability derivatives. *J. Chem. Phys.* **1977**, *66*, 2297−2305.
(35) Tuschel, D. Why are the Raman spectra of crystalline and amorphous solids different? *Spectroscopy* **2017**, *32*, 26−33.
(36) Challagulla, S.; Tarafder, K.; Ganesan, R.; Roy, S. Structure sensitive photocatalytic reduction of nitroarenes over TiO2. *Sci. Rep.* **2017**, *7*, No. 8783.
(37) Raz, E.; Lipson, S. G.; Polturak, E. Dendritic growth of ammonium chloride crystals: Measurements of the concentration field and a proposed nucleation model for growth. *Phys. Rev. A* **1989**, *40*, 1088−1095.
(38) Goto, M.; Oaki, Y.; Imai, H. Dendritic Growth of NaCl Crystals in a Gel Matrix: Variation of Branching and Control of Bending. *Cryst. Growth Des.* **2016**, *16*, 4278−4284.
(39) Weinberg, M. C. Surface nucleated transformation kinetics in 2- and 3-dimensional finite systems. *J. Non-Cryst. Solids* **1991**, *134*, 116−122.
(40) Li, T.; Bai-tong, L.; Fang, Z.-B.; Yin, Q.; Wang, R.; Liu, T. Integrating Active C3N4Moieties in Hydrogen-bonded Organic Frameworks for Efficient Photocatalysis. *J. Mater. Chem. A* **2021**, *9*, 4687−4691.

https://doi.org/10.1021/acsomega.3c04459
ACS Omega 2023, 8, 33831−33837